Journal of Power Sources 201 (2012) 10–17

Contents lists available at SciVerse ScienceDirect

Journal of Power Sources

journal homepage: www.elsevier.com/locate/jpowsour

# The electrochemical and thermodynamic characterization of $PrBaCo_{2-x}Fe_xO_{5+\delta}$ ($x = 0, 0.5, 1$) infiltrated into yttria-stabilized zirconia scaffold as cathodes for solid oxide fuel cells

Sihyuk Choi [a], Jeeyoung Shin [b], Guntae Kim [a,*]

[a] Interdisciplinary School of Green Energy, Ulsan National Institute of Science and Technology (UNIST), Ulsan 689-798, Republic of Korea
[b] Department of Mechanical Engineering, Dong-Eui University, Busan 614-714, Republic of Korea

ARTICLE INFO

*Article history:*
Received 5 August 2011
Received in revised form
27 September 2011
Accepted 29 September 2011
Available online 17 October 2011

*Keywords:*
Solid oxide fuel cells
Cathode
Double perovskite
Oxygen nonstoichiometry
Thermodynamic property
Electrochemical performance

ABSTRACT

The effect of Fe substitution for Co on the thermodynamic and electrical properties of the double perovskites, $PrBaCo_{2-x}Fe_xO_{5+\delta}$ (PBCF, $x = 0, 0.5, 1$), are investigated as cathode materials for intermediate-temperature solid oxide fuel cells (IT-SOFCs). At a given temperature, the electrical conductivity decreases with increasing Fe content, $x$, in the PBCF–YSZ composites in air. PBCF–YSZ ($x = 1$) composite appear to be more stable than PBCF–YSZ ($x = 0$) composite down to lower oxygen partial pressure, $p(O_2)$, at the same temperature. The higher oxidation enthalpies of the $x = 1$ composite can also explain the superior stability at roughly the same $p(O_2)$. The high entropy change for the $x = 1$ composite can indicate the high probability in the formation of interstitial oxygen at approximately the same $p(O_2)$. Impedance spectra of symmetrical cells (PBCF–YSZ/YSZ/PBCF–YSZ) show lower cathode polarization losses with increasing amounts of Fe. The maximum power densities of $x = 0$ composite and $x = 0.5$ composite are 0.68 and 0.72 W cm$^{-2}$, respectively, at 973 K. The maximum power density of the $x = 1$ composite is, however, about 20% higher than that of the other composites. Considering redox stability and electrochemical performance, higher Fe content of $PrBaCo_{2-x}Fe_xO_{5+\delta}$ ($x = 1$) is more suitable as a cathode material than $x = 0$ composite in IT-SOFC application.



## 1. Introduction

Fuel cells allow the direct conversion of chemically stored energy into electrical energy by means of electrochemical oxidation of various fuels. Solid oxide fuel cells (SOFCs) are considered to be among the most promising fuel cells. In SOFCs, an oxygen reduction reaction occurs at the cathode to produce oxygen anions, which then move through a dense oxygen-ion-conducting electrolyte to the anode. Current state-of-the-art technology SOFCs can produce electrical energy with very high efficiency, low emissions, and excellent fuel flexibility at high operating temperatures (>1273 K). High temperature can result, however, in a series of problems such as high cost, electrode sintering, interface reactions between cell components, and material compatibility challenges [1–5]. Much attention has consequently been directed toward lowering the SOFC working temperature to an intermediate level (773–1073 K) in order to resolve the aforementioned problems and allow the use of low-end interconnects and balance-of-plant materials as well. The operating temperature affects the oxygen kinetics, including oxygen surface absorption and ionic diffusivity. In intermediate-temperature SOFCs (IT-SOFCs), a critical problem is the poor activity of traditional cathode materials for electrochemical reduction of oxygen [4,5]. Current efforts are hence largely focused on finding appropriate cathode materials with low electrode resistance, good compatibility with the electrolyte, and other favorable chemico-physical properties suitable for IT-SOFCs applications [6–8].

Mixed ionic and electronic conductors (MIECs) containing Mn, Fe, Co, and Ni have been studied for use as cathode materials at intermediate operating temperature [9,10]. Among the various MIEC oxides, cobalt containing oxides such as $LaCoO_3$, (La, Sr)$CoO_3$, $BaCoO_3$, and (Ba, Sr)$CoO_3$ doped with transition metals have attracted strong interest owing to their high electrocatalytic activity for the oxygen reduction reaction (ORR). Recently, cobalt containing oxides such as $LnBaCo_2O_{5+\delta}$ (Ln = Pr, Nd, Sm, and Gd) with a cation ordered double perovskite-type structure have received widespread interest for their promising MIEC properties and potential application as IT-SOFC cathode materials [11–15].

The idealized crystal structure of a double perovskite is presented in Fig. 1. This family of compounds can be theoretically described with a stacking sequence of .../BaO/$CoO_2$/$LnO_x$/$CoO_2$... along the *C*-axis [16]. For example, all oxygen vacancies are localized at the rare earth layer $[Gd–O]_x$ in $GdBaCo_2O_{5+\delta}$. In this

* Corresponding author. Tel.: +82 52 217 2917; fax: +82 52 217 2909.
*E-mail address:* gtkim@unist.ac.kr (G. Kim).

0378-7753/$ – see front matter. 
doi:10.1016/j.jpowsour.2011.09.096

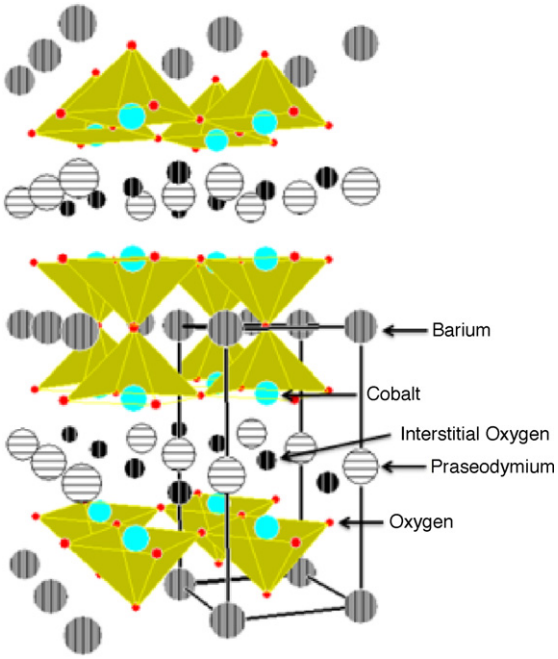


**Fig. 1.** The crystal structure of $PrBaCo_2O_{5+\delta}$.

structure, the Ba cations do not show a random distribution in the A site of the perovskite but tend to order in altering layers [17]. The particular distribution of vacancies in these materials could greatly enhance the diffusivity of oxide ions in the bulk of the material and may supply surface defect sites with enhanced reactivity toward molecular oxygen compared with non-ordered perovskites [18].

Among the various $LnBaCo_2O_{5+\delta}$ oxides, $GdBaCo_2O_{5+\delta}$ (GBCO) has been the most widely investigated material [13–15]. Its performance has been studied in conjunction with proton-conducting $BaZr_{0.1}Ce_{0.7}Y_{0.2}O_3$ electrolytes, $Sm_{0.2}Ce_{0.8}O_{19}$ (SDC), and yttria-stabilized zirconia (YSZ) [14]. Kim's group, however, reported that the bulk diffusion coefficient and surface exchange coefficient of $PrBaCo_2O_{5+\delta}$ (PBCO) could be 2–3 orders higher than those values of GBCO [19]. This suggests that PBCO material can provide superior fuel cell performance than GBCO as a cathode for IT-SOFCs. The Manthiram group reported the effects of Fe partially substituted for Co in $NdBaCo_2O_{5+\delta}$ (NBCO) in terms of oxygen content and electrical properties [20]. They noted that an increase of Fe leads to a decrease in the thermal expansion coefficient (TEC) and electrical conductivity because of the strong Fe–O bonds compared to Co–O bonds. Recently, the structure and electrochemical properties of a Fe doped layered structure perovskite, $PrBaCo_{2-x}Fe_xO_{5+\delta}$ ($x = 0$, 0.5, 1.0, 1.5, and 2.0), both as a powder bulk form and mixed powder with YSZ, were investigated. The authors reported that the $PrBaCo_{2-x}Fe_xO_{5+\delta}$ perovskites are not stable in the presence of YSZ even at temperature as low as 973 K [21]. Recent results, however, have shown that a composite electrode fabricated by infiltration of the electrode material into the YSZ backbone permits low sintering temperature, thereby avoiding solid state reaction [22–24]. The infiltration method has been widely used to prepare composite electrodes flexibly. This method allows the enlargement of the electrochemical reactive sites where the oxygen reduction reaction occurs, which could result in high performance of the composite electrode. This method can also provide a composite electrode with a uniform structure, because a conducting phase is added to the existing YSZ backbone, which leads to good conductivity [25,26].

Furthermore, most studies have focused on structure, electrochemical properties, and fuel cell performance of PBCO and $PrBaCoFeO_{5+\delta}$ (PBCF) oxides without a thorough understanding of their fundamental properties such as thermodynamic and electrical properties at the cathode operating condition, i.e., low oxygen partial pressure. To the best of our knowledge, the redox properties related with oxygen thermodynamics such as the oxidation enthalpies and entropies of PBCO–YSZ and PBCF–YSZ composites have never been reported. These properties can provide, however, critical information to determine the suitability of new electrodes prior to conducting fuel cell tests.

In this paper, through a comprehensive survey of cation ordered perovskite oxides, PBCO, having favorable properties for high fuel cell performance of IT-SOFCs, is chosen as a starting material. $PrBaCo_{2-x}Fe_xO_{5+\delta}$–YSZ composites are prepared by the infiltration method to assess the effects of Fe doping, and the microstructures of composites are characterized by X-ray powder diffraction (XRD) and field emission scanning electron microscopy (SEM). The electrical conductivities and redox properties of a $PrBaCo_{2-x}Fe_xO_{5+\delta}$–YSZ composite ($x = 0$ and 1.0) were measured simultaneously under a wide $p(O_2)$ range of 923–1023 K to evaluate the possibility of its use as a cathode material. Symmetric cell performance is measured to validate the potential of this new material as a cathode. The electrochemical performance of a $PrBaCo_{2-x}Fe_xO_{5+\delta}$–YSZ composite ($x = 0$, 0.5, and 1.0) single cell is also evaluated by producing a $PrBaCo_{2-x}Fe_xO_{5+\delta}$ infiltrated cathode on a Ni-YSZ anode-supported cell for application to IT-SOFCs.

## 2. Experimental

$PrBaCo_{2-x}Fe_xO_{5+\delta}$–YSZ composites ($x = 0$, 0.5, 1) were prepared for coulometric titration and electrical conductivity measurement by infiltrating $PrBaCo_{2-x}Fe_xO_{5+\delta}$ into porous YSZ. Porous YSZ slurries were made by mixing YSZ powder (Tosoh Corp., TZ-8Y), a dispersant (Rohm and Haas, Duramax3005), binder (Rohm and Haas, HA-12 and B1000), and pore former (Alfa Aeser, Graphite, 325 mesh) with distilled water. Slabs (2 mm × 2 mm × 10 mm) prepared from YSZ slurries were then sintered at 1773 K to produce a YSZ structure with a porosity of about 65%.

The $PrBaCo_{2-x}Fe_xO_{5+\delta}$ solution was prepared with stoichiometric amounts of $Pr(NO_3)_3{\cdot}6H_2O$ (Aldrich, 99.9%, metal basis), $Ba(NO_3)_2$ (Aldrich, 99+%), $Co(NO_3)_2{\cdot}6H_2O$ (Aldrich, 98+%), $Fe(NO_3)_3{\cdot}6H_2O$ (Aldrich, 98%), and citric acid in distilled water, and then infiltrated into the YSZ slab. The $PrBaCo_{2-x}Fe_xO_{5+\delta}$–YSZ composites were calcined in air at 723 K for 20 min to decompose nitrate ions and citric acid. This procedure was repeated until the desired 42 wt.% loading of oxide is achieved. Finally, these composites were calcined in air at 1023 K for 4 h to form a double perovskite phase.

The XRD (Rigaku diffractometer, Cu Ka radiation) patterns of the prepared samples were used to confirm the crystalline structure with a scan rate of $0.5^\circ\,min^{-1}$ and a range of $20^\circ < 2\theta < 60^\circ$. The microstructure of the cell was also examined using a SEM (Nova SEM). A thermogravimetric analysis (TGA) was carried out using a SDT-Q600 (TA instrument, USA). TGA experiments were performed from 373 to 1073 K with a heating/cooling rate of 3 K $min^{-1}$ in air.

The redox properties of the 42 wt.% $PrBaCo_{2-x}Fe_xO_{5+\delta}$–YSZ composites were measured using coulometric titration as a function of the oxygen partial pressure, $p(O_2)$. The samples for these experiments were fabricated by infiltration of the aqueous nitrate salts of $PrBaCo_{2-x}Fe_xO_{5+\delta}$ into a porous YSZ slab. The coulometric-titration rig, which has been explained in detail elsewhere, is simply a sealed YSZ tube with Ag-paste electrodes on both sides [22–24]. After purging 5% $O_2$–Ar gas over the sample in the tube for 24 h, $p(O_2)$ was determined from the open-circuit voltage (OCV). Oxygen could be added or removed from the tube by passing current through the same electrodes as used for the OCV sensor. The sample was allowed to equilibrate until the potential varied in a range of less than 1 mV $h^{-1}$. Oxygen nonstoichiometry was determined

through this procedure at 923, 973, and 1023 K over a wide range of oxygen partial pressure. Electrical conductivity was measured by a four-terminal DC arrangement simultaneously with a BioLogic Potentiostat.

Electrolyte support symmetrical cells were made by tape casting, with the outer two layers having pore formers in order to evaluate the intrinsic properties of the electrode. A dense YSZ slurry was prepared by mixing YSZ powder (Tosoh Corp., TZ-8Y) in distilled water, into which a dispersant (Rohm and Haas, Duramax3005) and binders (Rohm and Haas, HA-12 and B1000) were added. A porous electrode backbone was prepared by sequentially adding YSZ powder (Tosoh Corp., TZ-8Y), dispersant (Rohm and Haas, Duramax3005), binders (Rohm and Haas, HA-12 and B1000), and graphite (Alfa Aesar, UCP-2 grade) to distilled water. The porous–dense–porous YSZ structure was produced by lamination, followed by sintering at 1773 K for 4 h, after which the porosity was approximately 65%. The cathode materials were added onto both porous electrode backbones using an infiltration technique, which was repeated until the loading reached 45 wt.%, and the symmetrical cells were finally sintered at 1023 K. The detailed symmetrical cell procedure has been described elsewhere [27].

A Ni-YSZ anode-supported cell was used to evaluate the electrochemical performance of the composite cathode material in IT-SOFCs. The Ni-YSZ powder was prepared using nickel oxide (J. T. Baker), YSZ (Tosoh corp., TZ-8Y), and graphite (Aldrich, 20 μm) as a pore-former, and were then primarily mixed at 55:45:25 by weight and ball-milled together for 72 h in ethanol. The Ni-YSZ powder was dried in an oven for 24 h. This powder was pressed into pellets at 5 MPa and sintered in air at 1473 K for 3 h. To improve the performance of the cell, the anode functional layer was coated by dipping the anode support into mixed slurries of NiO-YSZ (60:40 wt.%) powder, isopropanol, and toluene followed by sintering at 1473 K for 3 h. The pellets were again coated by dense YSZ electrolyte layers through a dipping process and then sintered. A second layer of the YSZ electrolyte was added via dipping in order to prevent the formation of pin-holes, and a porous cathode backbone (thickness ~50 μm) was then laminated onto this layer. The thickness of the entire dense YSZ electrolyte layer was approximately 15 μm. The pellets, with an active electrode area of 0.36 $cm^2$, were finally sintered at 1773 K for 2 h under an air atmosphere. The cathode material was added into the porous YSZ cathode backbone by the infiltration technique, which was repeated until the loading reached 45 wt.%. Finally, the cell was sintered at the same temperature, 1023 K, as used for the preparation of slab samples.

Ag wires were attached to both electrodes using Ag paste as a current collector. The cells were fixed on a 10 mm diameter alumina tube using a ceramic adhesive (Aremco, Ceramabond 552). During the single cell test, humidified $H_2$ (3% $H_2O$) was supplied to the anode side with a flow rate of 20 mL $min^{-1}$ by first passing $H_2$ through a water bubbler, and the cathode was left exposed to the air. AC impedance spectra under 800 mV and *I–V* polarization curves were obtained at various currents in a frequency range of 1 mHz to 500 kHz and 14 mA AC perturbation using a BioLogic Potentiostat.

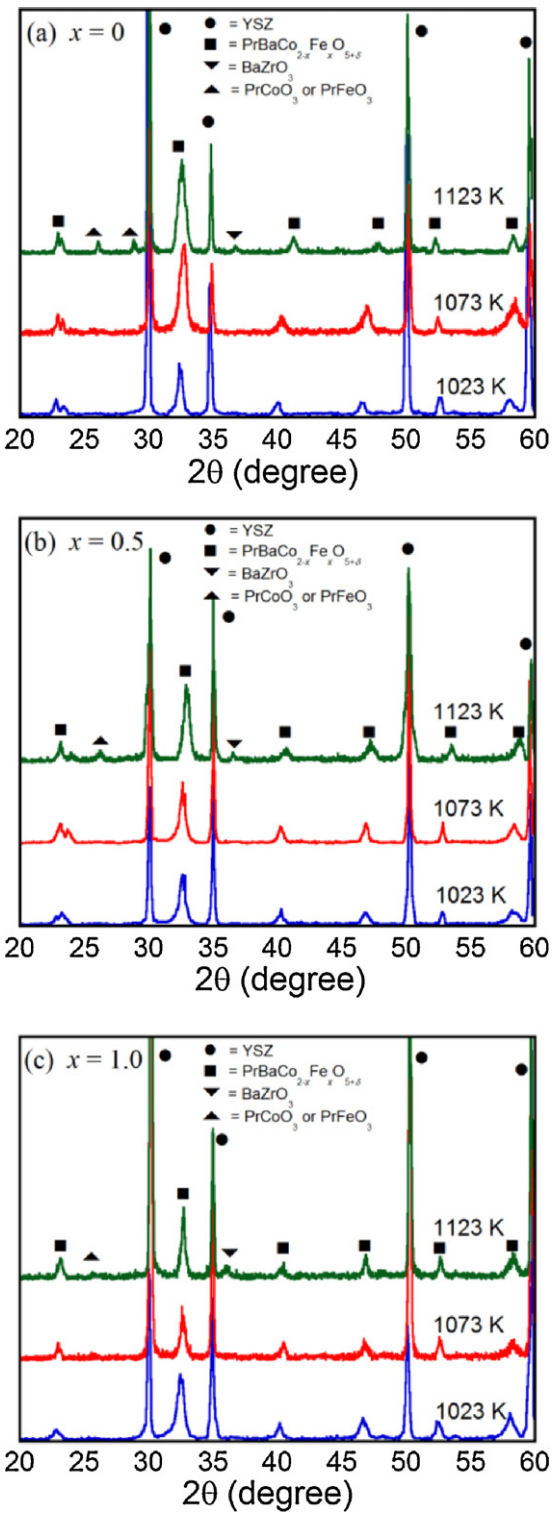


**Fig. 2.** The X-ray diffraction for $PrBaCo_{2-x}Fe_xO_{5+\delta}$–YSZ composites ($x$ = 0, 0.5, 1) formed by infiltration method after sintered at 1023, 1073, and 1123 K in air.

## 3. Results and discussion

The X-ray diffraction profile of 42 wt.% $PrBaCo_{2-x}Fe_xO_{5+\delta}$–YSZ composites ($x$ = 0, 0.5, 1) after calcination at 1023 K, 1073 K, and 1123 K are shown in Fig. 2. The XRD data show only peaks corresponding to $PrBaCo_{2-x}Fe_xO_{5+\delta}$ and YSZ, with no additional diffraction peaks under 1073 K. Beyond 1123 K, the data begin to show secondary phases such as $PrCoO_3$, $PrFeO_3$, and $BaZrO_3$. Therefore, the final sintering temperature of all experiments is determined as 1023 K. The XRD patterns are consistent with the formation of very small crystallites due to the infiltration procedure, which in turn causes adequate peak broadening by the unresolved two peaks.

SEM images of $PrBaCo_{2-x}Fe_xO_{5+\delta}$–YSZ composites ($x$ = 0, 0.5, 1) after calcination at 1023 K are presented in Fig. 3. A cross-section of the tri-layer (NiO-YSZ/YSZ/$PrBaCo_{2-x}Fe_xO_{5+\delta}$–YSZ composites) cell near the electrolyte before single cell tests is shown in Fig. 3(a).

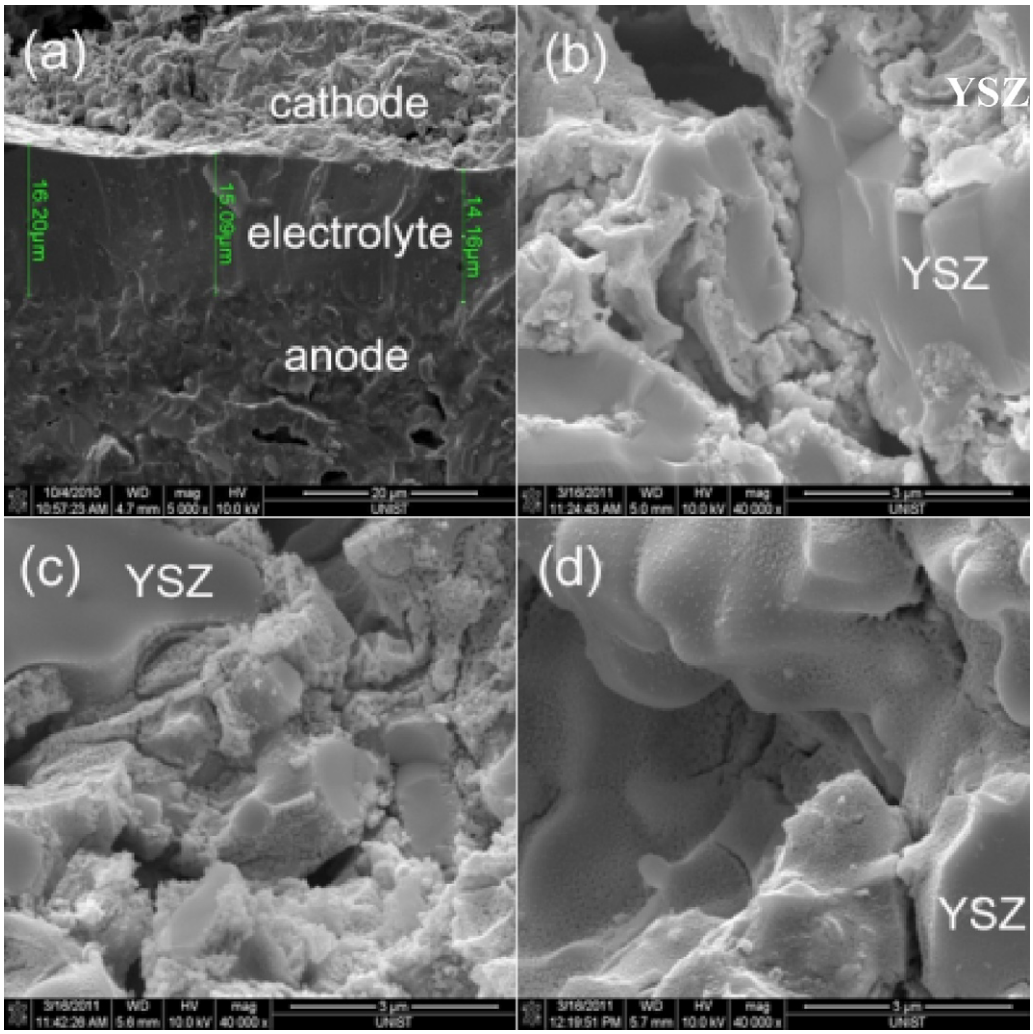


**Fig. 3.** SEM images showing the microstructure of the composites formed by infiltration method after calcined at 1023 K in air: (a) Cross-sectional of tri-layer cell before cell test and $PrBaCo_{2-x}Fe_xO_{5+\delta}$–YSZ composites, (b) $x = 0$, (c) $x = 0.5$, (d) $x = 1.0$.

The thickness of the YSZ electrolyte is approximately 15 μm and the cell is successfully fabricated without any pinholes, isolated voids or cracks. The PBCO particles are uniformly coated on the surfaces of the YSZ pores, as seen in Fig. 3(b). The uniform coating due to the good wettability of the oxide onto the YSZ is expected to result in good interconnection and, accordingly, enhanced electrical conductivity. The micrographs of Fe doped materials provided in Fig. 3(c) and (d) also indicate that the particle size decreases with an increase of Fe doping. This can be attributed to an increase of electrochemical reactive sites with higher amounts of Fe. The BET surface area measurement also confirm that the surface area of $PrBaCo_{2-x}Fe_xO_{5+\delta}$–YSZ composites ($x = 0$, 0.5, 1) are 0.78 $m^2\,g^{-1}$, 1.00 $m^2\,g^{-1}$, and 2.16 $m^2\,g^{-1}$, respectively. Therefore, the higher surface area can explain higher electrochemical reactive surface areas with increasing amounts of Fe, which leads to higher cell performance.

The variation of oxygen content of $PrBaCo_{2-x}Fe_xO_{5+\delta}$ ($x = 0$, 1) with temperature in air shows in Fig. 4. The initial oxygen content at 373 K was determined from the TGA in a hydrogen atmosphere of which values of $x = 0$ and 1 are 5.7 and 6.0, respectively. The samples begin to lose oxygen at 473 K due to loss of interstitial oxygen from the lattice. The PBCF oxide loses 0.2 oxygen atoms per formula unit upon heating to 1073 K and PBCO oxide loses 0.3 under the same conditions, because the Fe–O bonds are much stronger than the Co–O bonds [20,30].

An Arrhenius plot of the electrical conductivity of the 42 wt.% $PrBaCo_{2-x}Fe_xO_{5+\delta}$–YSZ composites ($x = 0$, 0.5, 1) in air is presented in Fig. 5. The samples show increase electrical conductivity with increasing temperature until 1123 K and a sudden drop thereafter. This drastic decrease may originate from the formation of

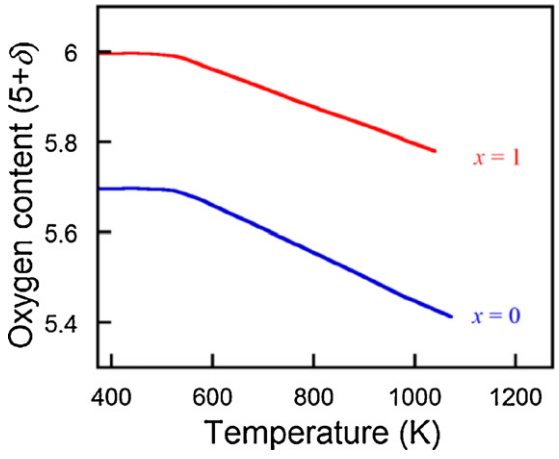


**Fig. 4.** Thermogravimetric data of $PrBaCo_{2-x}Fe_xO_{5+\delta}$ ($x = 0.1$) showing a variation of oxygen content as a function of temperature in air.

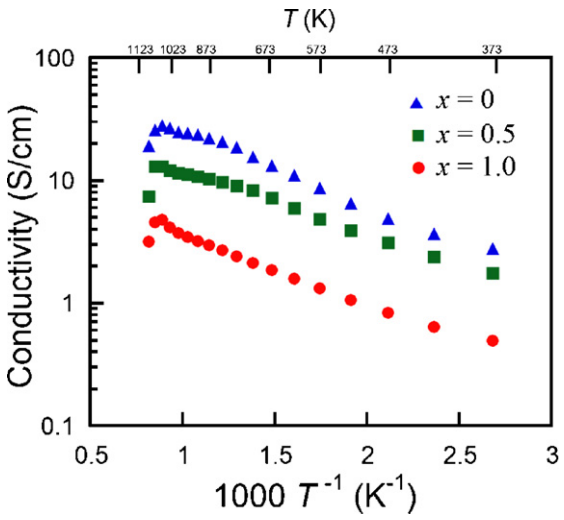


**Fig. 5.** Electrical conductivity data for $PrBaCo_{2-x}Fe_xO_{5+\delta}$–YSZ ($x = 0, 0.5, 1$) composites as a function of temperature in air.

a secondary phase such as $BaZrO_3$ from inter-diffusion between Zr in YSZ and Ba in the PBCO. The electrical conductivities of the bulk material [28], however, are reported to show an inflection point at a lower temperature as compared to $PrBaCo_{2-x}Fe_xO_{5+\delta}$–YSZ composites. This discrepancy is one of the reasons that bulk materials and composites should be treated differently. In addition, the interfacial interaction between the YSZ and samples may affect the electrical characteristics [22,23]. The electrical conductivities of PBCO–YSZ and PBCF–YSZ composites are not substantially different from those of $NdBaCo_{2-x}Fe_xO_{5+\delta}$–YSZ composites ($x = 0, 1$) [23].

The electrical conductivities of 42 wt.% PBCO–YSZ and PBCF–YSZ composites as a function of $p(O_2)$ in a temperature range of $923 < T(K) < 1023$ are presented in Fig. 6. Each measured datum point corresponds to an isotherm point in Fig. 7. The electrical conductivities of the PBCO–YSZ composite range from 18 to 23 S $cm^{-1}$ at various $p(O_2)$ but the electrical conductivities of the PBCF–YSZ composite are roughly one order of magnitude smaller than those of the PBCO–YSZ composite.

The electrical conductivities decrease with decreasing $p(O_2)$. This is in agreement with the findings of other studies, which report smaller electrical conductivities at lower $p(O_2)$ in fluorite layers due to the decrease concentration of mobile interstitial oxygen [29]. The predominant defects in $PrBaCo_{2-x}Fe_xO_{5+\delta}$ are the oxygen interstitials, $O_i''$, and the electronic holes, $h' = O_{O'}'$ [30]. Following the Kröger-Vink notation, the pseudo-chemical reaction can be regarded as the interaction between the defects and the atmosphere, as delineated in Eq. (1).

$$\frac{1}{2}O_2(g) + V_i^x + 2O_o^x \Leftrightarrow O_i'' + 2O_o' \quad (1)$$

The decrease in the interstitial oxygen concentration by lowering $p(O_2)$ results in a decrease in electronic holes; this can be explained in terms of electroneutrality, $2[O_i''] = [O_o']$. The decrease in electronic holes is finally responsible for the lower electronic conductivities at lower $p(O_2)$ [22].

The slope of electrical conductivity becomes steeper below $10^{-4}$ atm. This is consistent with the steeper slope of the isotherms at 973 K. A steeper slope may also be another sign of decomposition of the sample at low $p(O_2)$, which was also reported in previous studies [22,23]. This indicates that the decomposition begins to affect the electrical characteristics of the composites even before the decomposition process is completed. This behavior can be ascribed to the oxygen order–disorder phase transition at high temperature near this low $p(O_2)$ [31].

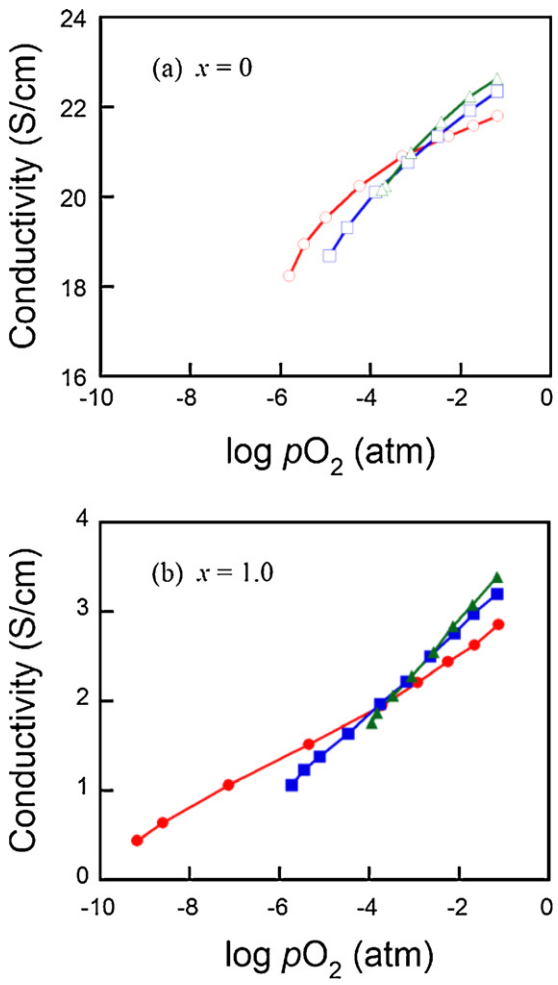


**Fig. 6.** The electrical conductivity of PBCO–YSZ composite at (○) 923 K, (□) 973 K, and (△) 1023 K and the electrical conductivity of PBCF–YSZ composite at (●) 923 K, (■) 973 K, and (▲) 1023 K in different oxygen partial pressures.

At a given temperature, electrical conductivity decreases with increasing Fe content $x$ in $PrBaCo_{2-x}Fe_xO_{5+\delta}$–YSZ composites, as found in other studies [20,23]. This can be explained by the preferential formation of $Fe^{4+}$ over $Co^{4+}$ for electronic charge compensation. Furthermore, the decreased covalency of the $Fe^{4+}$–O

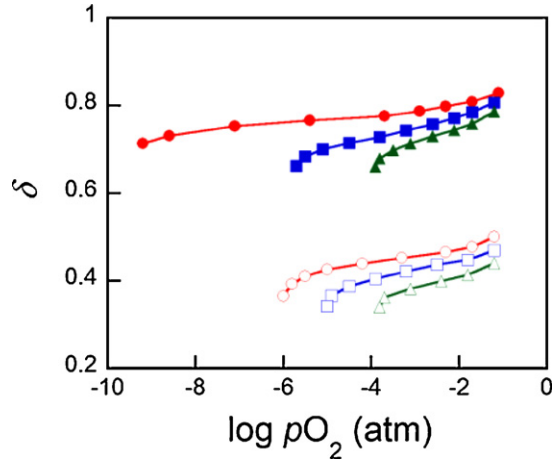


**Fig. 7.** Oxygen nonstoichiometry of PBCO–YSZ composite composites at (○) 923 K, (□) 973 K, and (△) 1023 K and PBCF–YSZ composite at (●) 923 K, (■) 973 K, and (▲) 1023 K by coulometric titration.

bond compared to the $Co^{4+}$–O bond can result in increased electron localization and decreased electrical conductivity with increasing Fe content [20].

The oxygen nonstoichiometry of the 42 wt.% $PrBaCo_{2-x}Fe_xO_{5+\delta}$–YSZ composites ($x = 0, 1$) in Fig. 7 are obtained as a function of $p(O_2)$ from 923 K to 1023 K by coulometric titration in order to characterize the redox properties of the PBCO and the PBCF composites. The initial oxygen content of the PBCO in air is 5.47 and that of the PBCF is determined as 5.81 at 973 K by TGA, as shown in Fig. 4. The oxidation isotherms for three different temperatures have similar shapes, suggesting that the reduction mechanisms of the composites are analogous. The gradient of the redox isotherms of both composites gradually becomes steeper until $10^{-4}$ atm $p(O_2)$ at 973 K according to a similar tendency. The isotherms of the PBCO–YSZ composite rapidly fall near this $p(O_2)$, which is possibly a starting point of decomposition. Those of the PBCF–YSZ composite, however, gradually decline to a lower $p(O_2)$. In other words, the PBCF–YSZ composites can be regarded as being more stable than the PBCO–YSZ composites at the same temperature. This stability is possibly a result of the stronger Fe–O bonds as compared to the Co–O bonds, as discussed earlier. Recently, oxygen nonstoichiometry of $NdBaCo_{2-x}Fe_xO_{5+\delta}$–YSZ composites ($x = 0, 1$) has been reported [23]. The report document thermodynamic behavior that is quite similar to the trends described in this study, and it was also shown that NBCF–YSZ has higher redox stability than a NBCO–YSZ composite due to partial substitution of Fe for Co, corresponding to the present study of $PrBaCo_{2-x}Fe_xO_{5+\delta}$–YSZ composites ($x = 0, 1$).

The higher redox stability is an important factor for stable electrochemical properties of a cathode material for IT-SOFCs at operating conditions. Consequently, the PBCF–YSZ composite is a more desirable cathode material for IT-SOFC applications in terms of redox stability.

The partial molar enthalpy and entropy of oxygen can be calculated by the slopes of isotherms. The equilibrium constant $K$, a function of $p(O_2)$ and Gibbs free energy $\Delta G$, is given by the following relation in Eq. (2)

$$\Delta G = -RT \ln K = \frac{1}{2} RT \ln p(O_2) \quad (2)$$

At constant $\delta$, the partial molar enthalpy of oxygen at various temperatures is shown by the Gibbs–Helmholtz equation.

$$\Delta H = \frac{\partial(\Delta G/T)}{\partial(1/T)} = \frac{R}{2} \frac{\partial \ln[p(O_2)]}{\partial(1/T)}|_{\delta} \quad (3)$$

And the partial molar entropy can be obtained by using the Maxwell relation as follows.

$$-\Delta S = \frac{\partial \Delta G}{\partial T} = \left(\frac{R}{2}\right)\left(\frac{\partial T \ln p(O_2)}{\partial T}\right)|\delta \quad (4)$$

The partial molar enthalpies of oxidation ($-\Delta H$) calculate by Eq. (3) for the PBCO–YSZ composites and PBCF–YSZ composites are shown in Fig. 8 as a function of $p(O_2)$. The partial enthalpies of oxidation range from −320 to −270 kJ mol$^{-1}$ for $p(O_2)$ between $10^{-4}$ and $10^{-2}$ atm in the case of the PBCO–YSZ composite, but the values of the PBCF–YSZ composite range from −550 to −250 kJ mol$^{-1}$ for $p(O_2)$ between $10^{-4}$ and $10^{-2}$ atm. The values of ($-\Delta H$) become lower for higher $\delta$, implying lower energy is needed for the formation of interstitial oxygen atoms. From this it can be hypothesized that the lattice structures near the defect sites become destabilized more easily as the oxidation of cobalt (Co) and/or iron (Fe) in the lattice proceeds [22,23]. Moreover, it can be confirmed again that the PBCF–YSZ composite is more stable than the PBCO–YSZ composite considering the higher oxidation enthalpy near the cathode operating condition. This result partially indicates that the oxidation

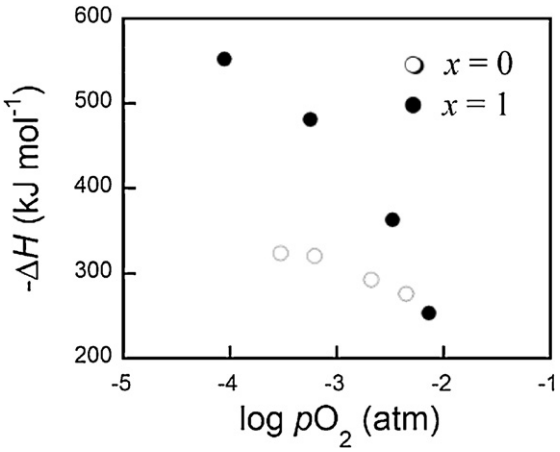


**Fig. 8.** Partial molar enthalpy of oxidation ($\Delta H$) of the PBCF–YSZ composites (●) and the PBCO–YSZ composites (○) composites at 973 K.

of PBCF–YSZ composite is comparatively difficult relative to that of PBCO–YSZ.

The partial molar enthalpies of oxidation of $NdBaCo_{2-x}Fe_xO_{5+\delta}$–YSZ composites ($x = 0, 1$) are studied recently [22,23]. The partial molar enthalpies range from −500 to −150 kJ mol$^{-1}$ for $p(O_2)$ between $10^{-5}$ and $10^{-2}$ atm (NBCO–YSZ composite) and −640 to −240 kJ mol$^{-1}$ for $p(O_2)$ between $10^{-5}$ and $10^{-2}$ atm (NBCF–YSZ composite). The enthalpy of NBCO–YSZ composite is higher than that of PBCO–YSZ composite, but the enthalpy of NBCF–YSZ composite is similar to that of PBCF–YSZ composite.

The partial molar entropies of oxidation ($\Delta S$), calculate from the differences of the Gibbs free energies and the enthalpies by Eq. (4), are shown in Fig. 9. It can be ascertained that the probabilities of the interstitial oxygen formation reaction itself decrease as excess oxygen increases. In other words, there are fewer sites for the interstitial oxygen formation reaction in the composites as the excess oxygen increases [22,23]. The higher partial molar entropies for PBCF–YSZ relative to those of PBCO–YSZ indicate that PBCF–YSZ has more available sites for interstitial oxygen formation reaction at the same $p(O_2)$ than PBCO–YSZ.

Typical impedance spectra for the symmetrical cells ($PrBaCo_{2-x}Fe_xO_{5+\delta}$–YSZ/YSZ/$PrBaCo_{2-x}Fe_xO_{5+\delta}$–YSZ) at 1023 K are displayed in Fig. 10. Impedance spectra of all compositions appear to be characterized by two pseudo semi-circles, which indicate interfacial resistance or ion and electron charge transfer at the higher frequency region and non-charge transfer such as a cathode reaction at

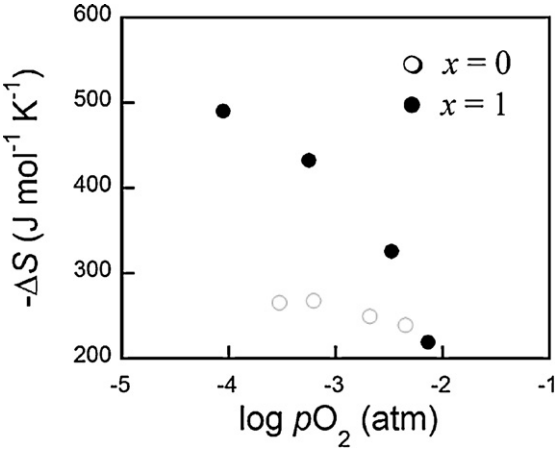


**Fig. 9.** Partial molar entropy of oxidation ($\Delta S$) of the PBCF–YSZ composites (●) and the PBCO–YSZ composites (○) composites at 973 K.

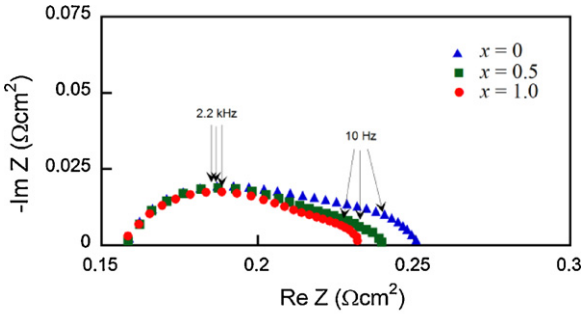


**Fig. 10.** Typical impedance spectra of the symmetrical cell ($PrBaCo_{2-x}Fe_xO_{5+\delta}$–YSZ/YSZ/$PrBaCo_{2-x}Fe_xO_{5+\delta}$–YSZ) measured under open-circuit condition at 973 K in air.

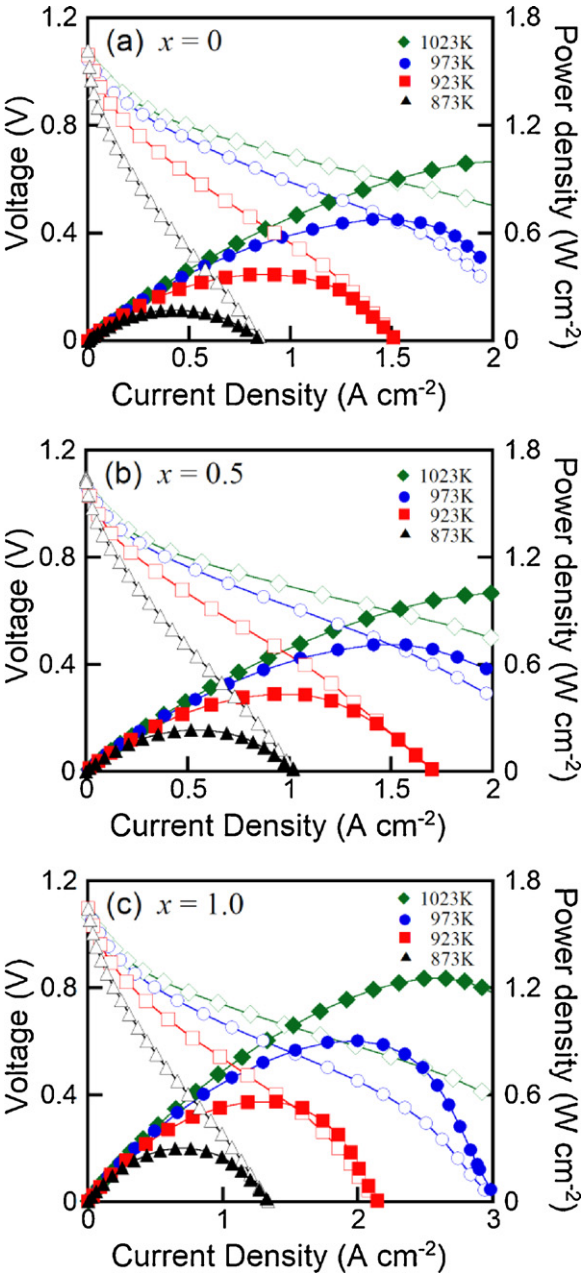


**Fig. 11.** *I–V* curves and corresponding power density curves of single cell (Ni-YSZ/YSZ/$PrBaCo_{2-x}Fe_xO_{5+\delta}$–YSZ) in various temperatures.

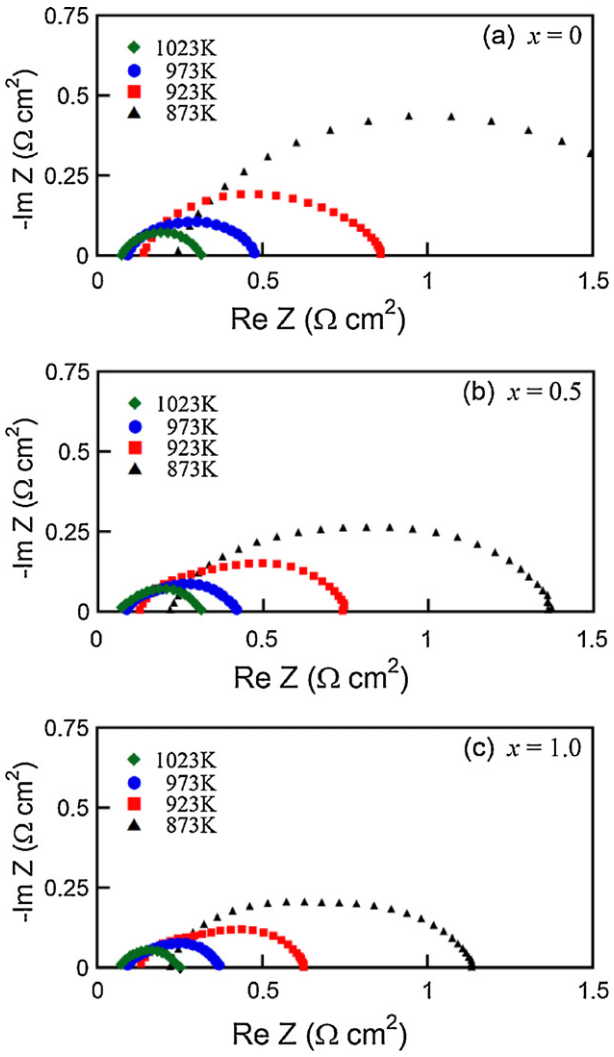


**Fig. 12.** Impedance spectra of the single cell (Ni-YSZ/YSZ/$PrBaCo_{2-x}Fe_xO_{5+\delta}$–YSZ) measured under 800 mV using $H_2$ (3% $H_2O$) as fuel and ambient air as oxidant in temperature range of 873–1023 K.

the lower frequency region [32]. The magnitude of the arcs at lower frequency decreases more than that of the arcs at higher frequency as the amount of Fe increases. This implies that oxygen surface exchange and gas-phase diffusion related to oxygen kinetics are key factors for electrochemical performance. The non-ohmic resistance of symmetrical cells with $x = 0$, 0.5, and 1 are 0.094 Ω cm², 0.083 Ω cm², and 0.075 Ω cm², respectively. Therefore, higher cell performance can be expected for cells with greater amounts of Fe.

The *I–V* curves and the corresponding power density of $PrBaCo_{2-x}Fe_xO_{5+\delta}$–YSZ composites ($x = 0$, 0.5, 1) shows in a range of 873–1023 K, with humidified $H_2$ (3% $H_2O$) as a fuel and static ambient air as an oxidant in Fig. 11. The OCVs are very close to the theoretical values from the Nernst potential predicted when the cells are well-sealed with a gas-tight electrolyte. The value is approximately 1.1 V at 973 K, and increases with decreasing operating temperature. The maximum power densities of the cell with the PBCO cathode material are 0.17, 0.37, 0.68, and 1.0 W cm$^{-2}$ at 873, 923, 973, and 1023 K, respectively, as seen in Fig. 11(a). The single cell performance is improved with partial substitution of Co with Fe ($x = 0.5$ and 0.1), as seen in Fig. 11(b) and (c). For example, the maximum power density of the PBCO composite is 0.68 W cm$^{-2}$ at 973 K and that of $PrBaCo_{1.5}Fe_{0.5}O_{5+\delta}$ is slightly higher at 0.71 W cm$^{-2}$ at the same temperature. The PBCF sample

exhibits much higher cell performance, 0.91 W cm$^{-2}$. This may be attributable to the extended electrochemical reactive sites as illustrated in relation to the microstructure of $PrBaCo_{2-x}Fe_xO_{5+\delta}$–YSZ composites in Fig. 2. In a recent paper, the electrochemical performances of $NdBaCo_{2-x}Fe_xO_{5+\delta}$–YSZ composites ($x = 0, 1$) is reported, with maximum power densities of 0.54 W cm$^{-2}$ and 0.67 W cm$^{-2}$ at 973 K, NBCO–YSZ and NBCF–YSZ composites, respectively [23]. This study of $PrBaCo_{2-x}Fe_xO_{5+\delta}$–YSZ composites, however, shows superior characteristics in terms of electrochemical performance (0.68 and 0.91 W cm$^{-2}$ at 973 K).

The electrochemical impedance spectra of NiO/YSZ/$PrBaCo_{2-x}Fe_xO_{5+\delta}$–YSZ cells ($x = 0$, 0.5, 1) under 800 mV through a temperature range of 873–1023 K are presented in Fig. 12. The ohmic resistance of the cell corresponds to the high frequency intercept, whereas the low frequency intercept corresponds to the total impedance of the cell. Therefore, the difference between the high frequency and low frequency intercepts with the real axis gives the non-ohmic resistance of the cell, including the anode and cathode–electrolyte interface resistance. A significant decrease of the non-ohmic resistance of the PBCO–YSZ composite is observed: 1.59, 0.72, 0.39, and 0.24 Ω cm$^2$ at 873, 923, 973, and 1023 K, respectively. It is clear that increased operating temperature leads to a considerable reduction of the non-ohmic resistance due to the faster oxygen reduction kinetics. The non-ohmic resistance also decreases with the substitution of Fe from 0.39 (PBCO–YSZ composite) down to 0.28 Ω cm$^2$ (PBCF–YSZ composite) at 973 K, leading to higher cell performance due to the extended electrochemical reactive sites. Since the electrical conductivity value of $x = 1$ sample is 3 S cm$^{-1}$, it can be considered that the electrical conductivity is not a limiting factor for the electrochemical performance if the thickness of electrode is less than 50 μm. Therefore, in terms of redox stability and cell performance, the PBCF–YSZ composite is a preferable candidate cathode material over the PBCO–YSZ composite in IT-SOFC applications.

## 4. Conclusions

Layered $PrBaCo_{2-x}Fe_xO_{5+\delta}$ oxides ($x = 0$, 0.5, 1) have been investigated as a cathode material for IT-SOFC application. The electrical conductivity of $PrBaCo_{2-x}Fe_xO_{5+\delta}$–YSZ composites in air decreases with higher Fe content, showing a sudden decrease at around 1123 K. The different redox properties of the composites are evaluated by coulometric titration. The PBCF–YSZ composite is revealed to be more stable than the PBCO–YSZ composite down to a lower $p(O_2)$. The higher oxidation enthalpies of the PBCF–YSZ composite can also explain their superior stability. The high entropy change for the PBCF–YSZ composite can indicate the high probability for the formation of interstitial oxygen at the same $p(O_2)$.

Typical impedance spectra for the symmetrical cells ($PrBaCo_{2-x}Fe_xO_{5+\delta}$–YSZ/YSZ/$PrBaCo_{2-x}Fe_xO_{5+\delta}$–YSZ) demonstrate lower cathode polarization losses leading to higher cell performance with higher amounts of Fe. An anode-supported cell based on a 15 μm YSZ electrolyte has been fabricated by infiltrating $PrBaCo_{2-x}Fe_xO_{5+\delta}$ into a porous YSZ as a cathode. The maximum power densities of the PBCO and $PBC_{1.5}F_{0.5}$ composites are fairly similar at 0.70 W cm$^{-2}$ at 973 K with $H_2$ as a fuel. The power density of the PBCF–YSZ composite is, however, higher than that of the other samples, possibly due to the extended electrochemical reactive sites.

Even though the conductivity of the PBCF–YSZ composite is lower than that of the PBCO–YSZ composite, the PBCF–YSZ composite is a more desirable candidate cathode material in IT-SOFC applications in terms of redox stability and cell performance.

## Acknowledgements

This research was supported by the WCU (World Class University) program (R31-2009-000-20012-0) and Mid-career Researcher Program (2011-0010773) through the National Research Foundation of Korea, funded by the Ministry of Education, Science and Technology.

## References

[1] B.C.H. Steele, A. Heinzel, Nature 414 (2001) 345–352.
[2] S.D. Park, J.M. Vohs, R.J. Gorte, Nature 404 (2000) 265–267.
[3] Z.P. Shao, S.M. Haile, J. Ahn, P.D. Ronney, Z.L. Zhan, S.A. Barnett, Nature 435 (2005) 795–798.
[4] N.P. Brandon, S. Skinner, B.C.H. Steele, Annu. Rev. Mater. Res. 33 (2003) 183–213.
[5] B.C.H. Steele, in: U. Bossel (Ed.), Proceedings of the First European Solid Oxide Fuel Cell Forum, European SOFC Forum, Oberrohrdorf, Switzerland, 1994, p. 375.
[6] A.J. Jacobson, Chem. Mater. 22 (2010) 660.
[7] Q.L. Ma, R.R. Peng, Y.J. Lin, H.F. Gao, G.Y. Meng, J. Power Sources 161 (2006) 95–98.
[8] Y.Y. Huang, J.M. Vohs, R.J. Gorte, J. Electrochem. Soc. 151 (2004) A646–A651.
[9] E.P. Murray, M.J. Sever, S.A. Barnett, Solid State Ionics 148 (2002) 27–34.
[10] S.J. Skinner, J.A. Kilner, Solid State Ionics 135 (2000) 709–712.
[11] G. Kim, S. Wang, A.J. Jacobson, Z. Yuan, W. Donner, C.L. Chen, L. Reimus, P. Brodersen, A.A. Mims, Appl. Phys. Lett. 88 (2006) 024103.
[12] D. Chen, R. Ran, K. Zhang, J. Wang, Z. Shao, J. Power Sources 188 (2009) 96–105.
[13] A.M. Chang, S.J. Skinner, J.A. Kilner, Solid State Ionics 177 (2006) 2009–2011.
[14] A. Tarancon, A. Morata, G. Dezanneau, S.J. Skinner, J.A. Kilner, S. Estrade, F. Hernandez-Ramirez, F. Peiro, J.R. Morante, J. Power Sources 174 (2007) 255–263.
[15] B. Lin, S.Q. Zhang, L.C. Zhang, L. Bi, H.P. Ding, X.Q. Liu, J.F. Gao, G.Y. Meng, J. Power Sources 177 (2008) 330–333.
[16] A. Maignan, C. Martin, D. Pelloquin, N. Nguyen, B. Raveau, J. Solid State Chem. 142 (1999) 247–260.
[17] T. Albert, J. Skinner, J. Richard, F. Chater, Hernandez-Ramirez, J.A. Kilner, J. Mater. Chem. 17 (2007) 3175–3181.
[18] A.A. Taskin, A.N. Lavrov, Y. Ando, Appl. Phys. Lett. 86 (2005) 091910.
[19] G. Kim, S. Wang, A.J. Jacobson, L. Reimus, P. Brodersen, C.A. Mims, J. Mater. Chem. 17 (2007) 2500–2505.
[20] Y.N. Kim, J.H. Kim, A. Manthiram, J. Power. Sources 195 (2010) 6411–6419.
[21] L. Zhao, J. Shen, B. He, F. Chen, C. Xia, Int. J. Hydrogen Energy 36 (2011) 3658–3665.
[22] S. Yoo, J.Y. Shin, G. Kim, J. Mater. Chem. 21 (2011) 439–443.
[23] S. Yoo, J.Y. Shin, G. Kim, J. Electrochem. Soc. 158 (2011) B632–B638.
[24] S. Sengodan, H.J. Yeo, J.Y. Shin, G. Kim, J. Power Sources 196 (2011) 3083–3088.
[25] G. Kim, J.M. Vohs, R.J. Gorte, J. Mater. Chem. 18 (2008) 2386–2390.
[26] S. Lee, M. Bevilacqua, P. Fornasiero, J.M. Vohs, R.J. Gorte, J. Power Sources 193 (2009) 747–753.
[27] W. Wang, M.D. Gross, J.M. Vohs, R.J. Gorte, J. Electrochem. Soc. 154 (2007) B439–B445.
[28] K. Zhang, L. Ge, R. Ran, Z. Shao, S. Liu, Acta Mater. 56 (2008) 4876–4889.
[29] F. Mauvy, J.M. Bassat, E. Boehm, J.P. Manaud, P. Dordor, J.C. Grenier, Solid State Ionics 158 (2003) 17–28.
[30] V.V. Vashook, S.P. Tolochko, I.I. Yushkevich, L.V. Makhnach, I.F. Kononyuk, H. Altenburg, J. Hauck, H. Ullmann, Solid State Ionics 110 (1998) 245–253.
[31] T. Nakamura, K. Yashiro, J. Mizusaki, Solid State Ionics 180 (2009) 368–376.
[32] S. Adler, J.A. Lane, B.C.H.J. Steele, J. Electrochem. Soc. 143 (1996) 3554–3564.